AD-A092 705 PHOTOMETRICS INC LEXINGTON MA F/G 22/2
DATA ANALYSIS OF FILM FROM AFGL ROCKET A31.603.(U)
AUG 79 M T CHAMBERLAIN F19628-79-M-0010
UNCLASSIFIED PHM-03-79 AFGL-TR-79-0195 NL

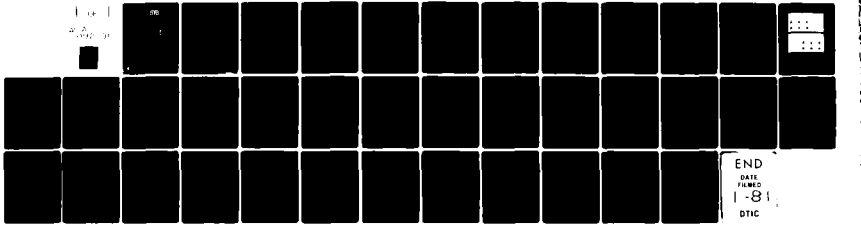

END
DATE FILMED
1-81
DTIC

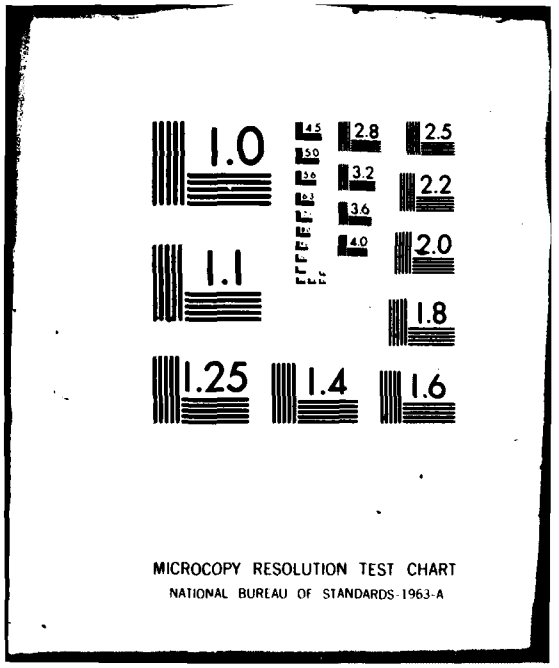
1.0
1.1
1.25
1.4
1.6
1.8
2.0
2.2
2.5
2.8
3.2
3.6
4.0
MICROCOPY RESOLUTION TEST CHART
NATIONAL BUREAU OF STANDARDS-1963-A

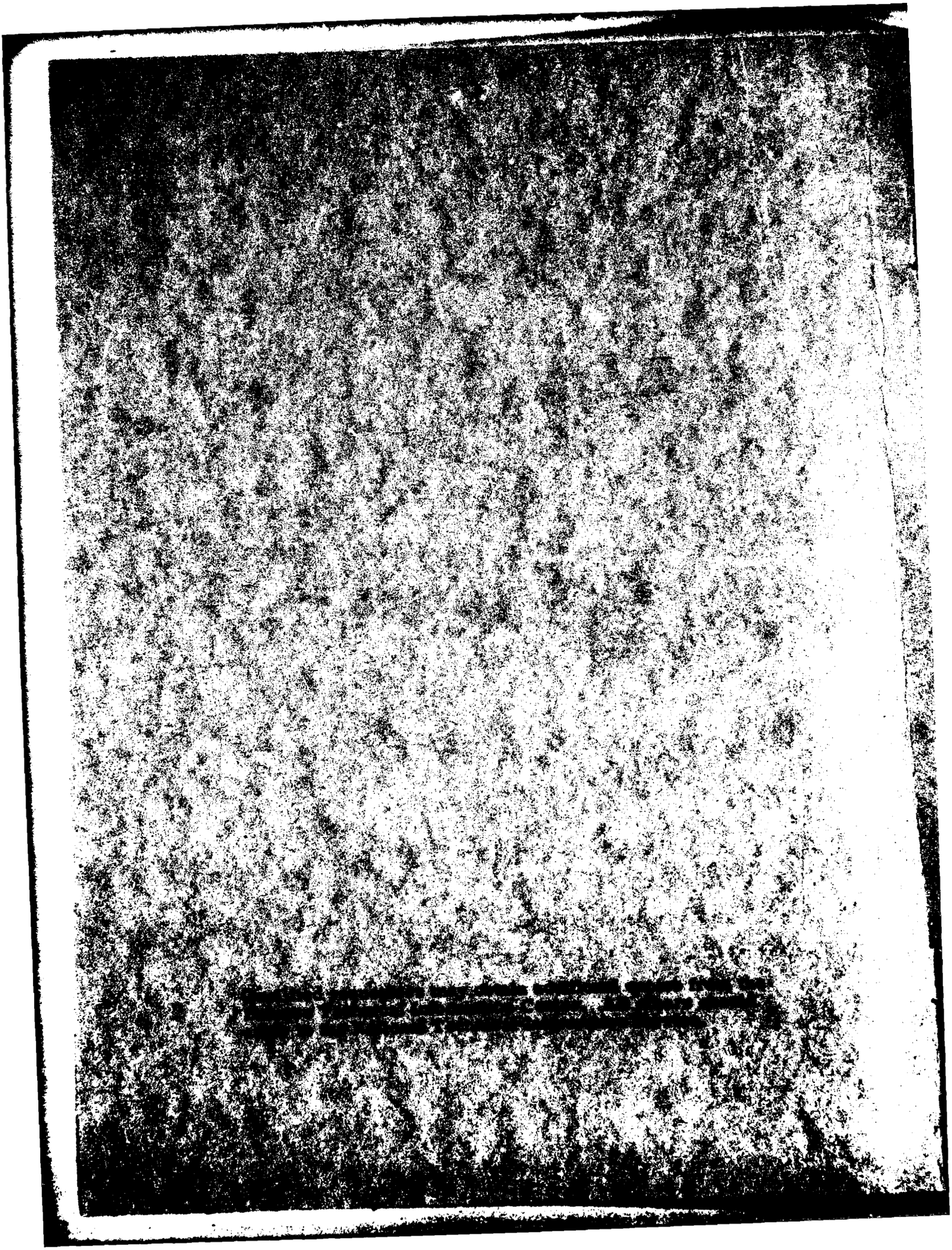

Unclassified

SECURITY CLASSIFICATION OF THIS PAGE (When Data Entered)

REPORT DOCUMENTATION PAGE	READ INSTRUCTIONS BEFORE COMPLETING FORM
1. REPORT NUMBER: AFGL-TR-79-0195	2. GOVT ACCESSION NO.: AD-A077 305
3. RECIPIENT'S CATALOG NUMBER:	
4. TITLE (and Subtitle): DATA ANALYSIS OF FILM FROM AFGL ROCKET A31.603	5. TYPE OF REPORT & PERIOD COVERED: Final 1 July 79 - 30 Sep 79
	6. PERFORMING ORG. REPORT NUMBER: PhM-03-79
7. AUTHOR(s): Malcolm T. Chamberlain	8. CONTRACT OR GRANT NUMBER(s): F19628-79-M-0010
9. PERFORMING ORGANIZATION NAME AND ADDRESS: PhotoMetrics, Inc. 442 Marrett Rd Lexington, MA 02173	10. PROGRAM ELEMENT, PROJECT, TASK AREA & WORK UNIT NUMBERS: 62101F 766109AA
11. CONTROLLING OFFICE NAME AND ADDRESS: Air Force Geophysics Laboratory Hanscom AFB, Massachusetts 01731 Monitor: Herbert A. Cohen/PHG	12. REPORT DATE: 20 August 1979
	13. NUMBER OF PAGES: 36
14. MONITORING AGENCY NAME & ADDRESS (if different from Controlling Office)	15. SECURITY CLASS (of this report): Unclassified
	15a. DECLASSIFICATION/DOWNGRADING SCHEDULE

16. DISTRIBUTION STATEMENT (of this Report)

Approved for public release; distribution unlimited.

17. DISTRIBUTION STATEMENT (of the abstract entered in Block 20, if different from Report)

18. SUPPLEMENTARY NOTES

19. KEY WORDS (Continue on reverse side if necessary and identify by block number)

Spacecraft Charging
Electrical Discharges
Ionsophere
Photographic Photometry

20. ABSTRACT (Continue on reverse side if necessary and identify by block number)

The film from the 16 mm camera onboard AFGL spacecraft-charging experiment rocket A31.603 (21 Jan 1978) was reviewed and analyzed to identify coincidence of frames with operation of the rocket's ion and electron acoelerators, determine payload aspect and rotation rate, and assess the intensity of fluorescent and other optical radiations from the

DD FORM 1 JAN 73 1473 EDITION OF 1 NOV 65 IS OBSOLETE

Unclassified

SECURITY CLASSIFICATION OF THIS PAGE (When Data Entered)

20. Abstract (continued)

plasma surrounding the vehicle and the vehicle surface. Upper limits determined for the radiance and volume emission rate of glows excited near the rocket were compared with theoretical predictions.

TABLE OF CONTENTS

LIST OF ILLUSTRATIONS

LIST OF TABLES

SECTION I

OVERVIEW OF THE DATA ANALYSIS

This report describes analysis of the film data from a split field automatic 16 mm camera system flown on AFGL rocket A31.603 from white Sands Missile Range NM on 21 Jan 1978. The objective of the camera was to measure by photographic photometry the surface brightness distribution of luminous electrical discharges in the plasma surrounding the rocket charged with respect to the ambient ionospheric plasma, and also to record arcing between parts of the rocket payload at different potentials. The work was part of an experiment by the Air Force Geophysics Laboratories (LKB Branch) on spacecraft charging at F-region altitudes. The rocket experiment and camera system are described in Ref 1.

Positive and negative charging with respect to the surrounding plasma was achieved by emitting programmed beams of ~2 keV Xe^+ ions and electrons from the rocket (refer to Table 2 of Ref 1 for beam currents and accelerating voltages). The camera functioned somewhat differently from planned, supposedly due to electronic interference by high voltage pulses from the ion accelerator. Its time sequencing was not immediately obvious from the preliminary examination of the film. Hence some further effort was needed to coordinate the film data with the telemetered data on beam currents and rocket potential.

The preliminary examination of the film (Section III of Ref 1) showed no readily-detectable evidence of any luminosity in either segment of the camera's field of view beyond scattered moonlight in the forward direction and reflections of moonlight from the payload surface. It was necessary to determine the actual timing of the camera before attempting to relate in more detail the film density distribution to vehicle potential or accelerator operation. We therefore have carefully re-examined the film and the data on camera

pulsing (also part of the telemetry record), and identified each frame unambiguously. Developed densities on selected frames were then measured by scanning microdensitometry to search for evidence of beam plasma discharge in the payload sheath and particle excited fluorescence on the payload skin. Upper limits are set for intensities of radiation excited by these mechanisms, and supporting calculations were made of theoretically expected volume emission rates in the sheath for various amounts and scenarios of xenon ions, ambient ions and/or electrons traveling through the sheath to the payload surface.

In addition timing of lunar reflections from the payload skin has been used to infer the vehicle aspect during flight. This was required to reduce ambiguities in aspect information provided by the onboard magnetometers.

SECTION II

FILM ANALYSIS

PREVIOUS DOCUMENTATION

A preliminary review of the photographic data is presented in Ref 1. Complete design and engineering particulars of the camera system, including operating and diagnostic procedures, are given in the Equipment Information Report submitted in Nov 1977 (Ref 2). Some description of the camera control procedure and method for labeling the frames is included in Ref 3. A critical review of the considerations leading to the specific design, and of performance in ground tests of the realized instrument, was submitted in the Design Evaluation Report (Ref 4).

FILM FRAME IDENTIFICATION

Synchronization between the camera and the ion and electron accelerators was determined by comparing the film, frame by frame, with printed lists of telemetry records of the accelerator operation. Coded numbers representing the mode of operation of the ion and electron accelerator and the program cycle had been placed on the film during the flight. (These numbers were intended to provide a unique identification for every frame but, as neither the camera or the accelerators themselves functioned exactly as planned, this was not the case.) The MODE numbers were compared with a listing of experimental parameters (not included in this report) in which the accelerator mode had been derived from analog chart of the on-board programmer voltage staircase (telemetry mainframe word 15).

The CYCLE number encoded on the film was incorrectly described in Ref 2, page 16. Its behavior tended to follow the description in Ref 3 (p 57 ff), but was so erratic that it could not be reliably used as an aid to frame identification. However every frame on the film could be readily identified by matching the coded MODE

numbers with the accelerator modes (as shown on the list), bringing the program sequence on the two records into synchronism. The possibility of a systematic error in coding of numbers on the film, which could have led to displacement of the film record with respect to other records, was removed by the occurrence of an occasional very short exposure when the electrodes in the camera's field of view were illuminated by the moon. The resulting low image density identified the short film exposure, which in each case agreed with the listing. The film frame list is given in Appendix A with results of film density measurements described later.

CAMERA MALFUNCTION

The camera operated as programmed for the first 93 sec after camera turn-on at 94 sec after launch, except for a few periods when it ran in cine mode after pulsing. After the data frame at 186.962 sec there were usually two frames for each MODE number on the film, and in addition often several digits of the CYCLE number were blank, usually in the first frame of each pair. Each frame, or pair of frames, could nonetheless be identified, but as there was no way to determine the exposure duration of each frame when they appeared in pairs this section of the film was generally not considered when searching for optical emissions.

The telemetry record showed that the camera battery voltage dropped to near zero volts for about $\frac{1}{4}$ sec at time 32587.967Z or flight time 186.967 sec, i.e. at the time of the change in character of the film record. Post-flight inspection showed some badly burnt components in the camera's speed-limiting optical tachometer. It is now believed that a short in this circuit caused the severe momentary drop in battery voltage.

Examination of the camera indicated that the damaged tachometer allowed the film advance and shutter mechanism to run so fast that it

could not stop after advancing just one frame as required. Actual cause of the component failure has not yet been determined.

PAYLOAD ATTITUDE

Semi-specular reflections of the moon from the payload skin in the vicinity of the electrodes mounted on the insulating ring were used to obtain information about payload orientation during flight. The rocket was believed to be tumbling end-over-end and was also understood to roll very slowly about its longitudinal axis. Four separate sequences of lunar reflections were photographed on the payload skin at various times during the flight. The overall timing between sequences was irregular but within each sequence the reflection point (highest scene brightness) was seen to move in a regular fashion around the payload, indicating a slow spin about the axis. This can bee seen in Figure 1. At the time of the flight the lunar disc was 92% illuminated and was at elevation 37°, azimuth 272.3°.

At four times during the flight, i.e. once during each of the sequences mentioned above, a reflection was recorded approximately centered on the electrodes as in the frame numbered 01.0000 in Figure 1. The line from the central electrode pair to the mirror by which the camera viewed the skin was at 37° to the rocket surface, and therefore at those times the rearward vehicle axis would have been pointing 37° away from the moon if the rocket surface were indeed producing truce specular reflection. The vehicle axis would then have been somewhere on a cone of half-angle 37° about the direction vector to the moon and the vehicle's forward axis, at the four times shown in Table 1, on a cone of 37° semi-angle having a direction elevation -34°, azimuth 92.3°.

Examination of the rocket surface in the vicinity of the insulating separator containing the electrodes showed fine circumferential

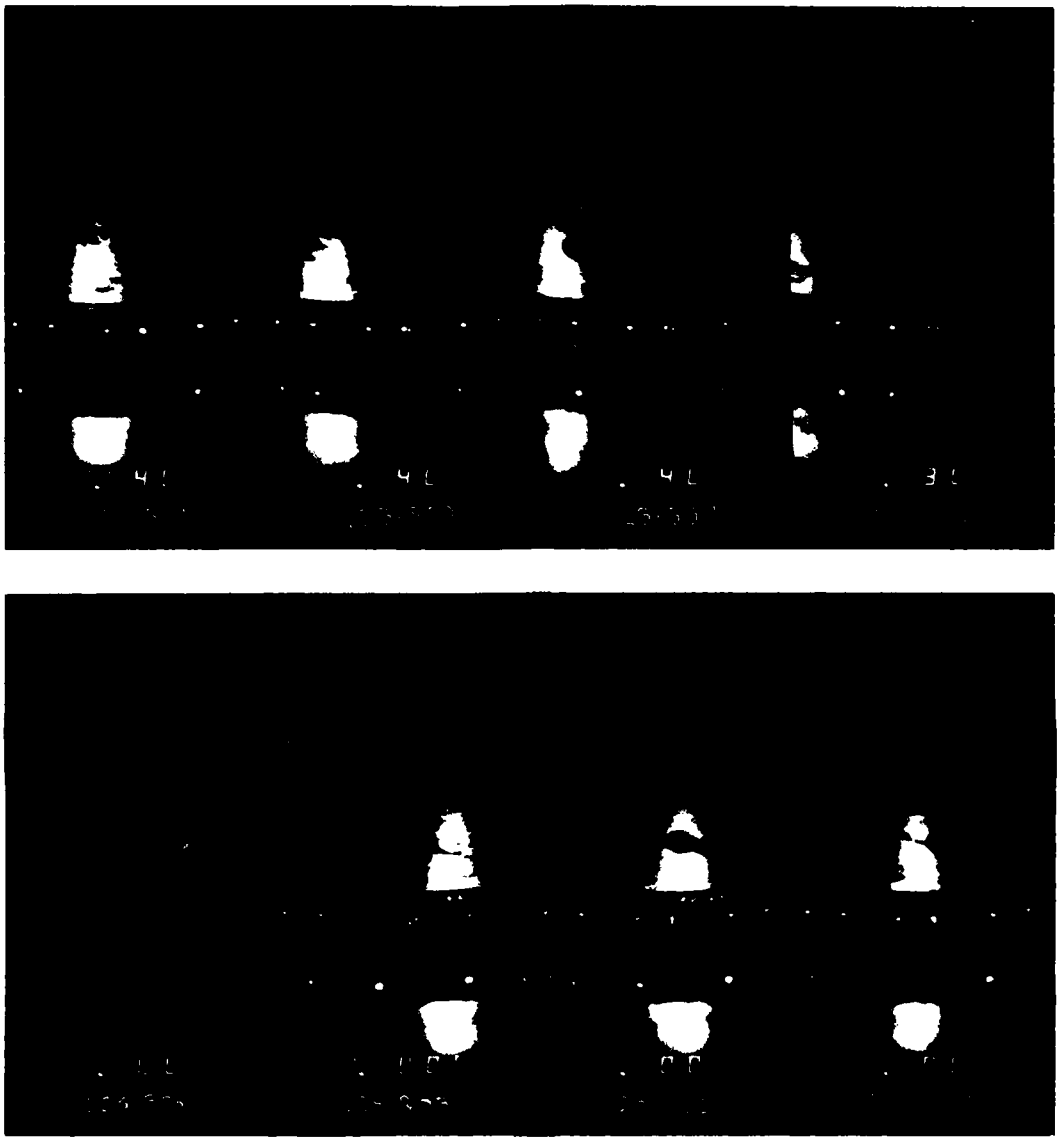

Figure 1. Sequence of consecutive film frames showing lunar reflections on the rocket surface, to determine payload rotation rate from angular rate of progression of reflections. The frame marked 01.0000 is the first entry in Table 1 and was used to infer payload aspect information at time of that exposure. Time from launch, in seconds of start of corresponding experiment program mode has been added below the MODE. CYCLE coding at the bottom of each frame.

machining marks. Reflection of a point, or nearly point, source of light from such a surface is not a well defined spot as would be seen on a smooth surface but a line of reflections, one from each groove, running over a considerable length of the cylinder. As the observed reflections were limited in this case by the camera field of view rather than the geometry of the reflections it is not possible here to locate the moon, with respect to the rocket, any better than to say that, at the times in Table 1, it was in the plane quadrant defined by the rocket's rearward axis and radius vector through the mirror mount.

Such reflections were recorded during accelerator modes starting at times 124.839, 159.300, 265.936 sec, and between the modes starting at 405.837 and 406.329 sec. These modes were of duration t = 463, 468, 390 and 490 millisec respectively. The corresponding shutter opening was later than the mode change by the 40 millisec taken for film advance so that the mid-point (in Table 1) of these exposures would be $40 + \frac{t - 40}{2}$ millisec later than the nominal starting times listed above.

Table 1. Mean times for film exposures showing lunar reflections at central electrode pairs on rocket surface, with film frame identification and magnetic pitch angle of the rocket's longitudinal axis

Adjacent Footage Numbers	Code	Rocket Time, sec	Universal Time, 21 Jan 78	Magnetic Pitch Angle
51346-45	01.0000	125,091	32526.091	65.6°
51341-40	01.0100	159.554	32560.554	36.8°
51323-22	02.0300	266.151	32667.151	36.7°
51301-00	11.0400 12.0400	406.348	32807.348	21.2°

Payload rotation rate was determined from the sequence of film frames in Figure 1, showing reflections of the moon on the vehicle skin. Estimates were made of the distance x of successive reflections around the payload surface from the central electrode pair. The geometry of the imagery is shown in Figure 2. The viewing mirror M is a distance h above the surface of the rocket which has radius r, and reflections were recorded at position S on the surface. The angle β is the rocket rotation angle, calculated from the following -:

$$\Theta = x/r \text{ radians}$$

$$\overline{MS} = [r^2 + (r + h)^2 - 2r(r + h)\cos\Theta]^{\frac{1}{2}}$$

$$\alpha = \sin^{-1}[r/\overline{MS} \sin\Theta] \text{ radians}$$

$$\beta = (\Theta + \alpha) \text{ radians.}$$

The mid point for each exposure was taken to be $t_s + 0.04 + \frac{t - 0.04}{2}$ sec, where t_s is the starting time of the appropriate program mode and t is the duration of that mode. This expression accounts for the delay between mode change and shutter opening and also for the loss of ~40 millisec observing time during film advance.

A linear least squares fit to a plot of β vs time gave a slope, or rotation rate, of 0.091 ± 0.006 radians sec^{-1}. This is 0.014 ± 0.001 revolutions sec^{-1} or about 1 revolution every 71 seconds with a precision of the order of 7%.

Rotation rate derived from the y-magnetometer data was 1/23 sec^{-1}. The disagreement between this figure and the one derived from the optical data may be due in part to the other components of the vehicle motion, e.g. tumbling. Figure 2 is a projection of the ray paths onto a plane normal to the rocket axis and thus does not fully describe the 3-D geometry of the reflections. If the magnetometer-derived rotation rate is assumed to be correct and the reflection geometry considered in a full three-dimensional representation further information relating to vehicle aspect might be obtainable.

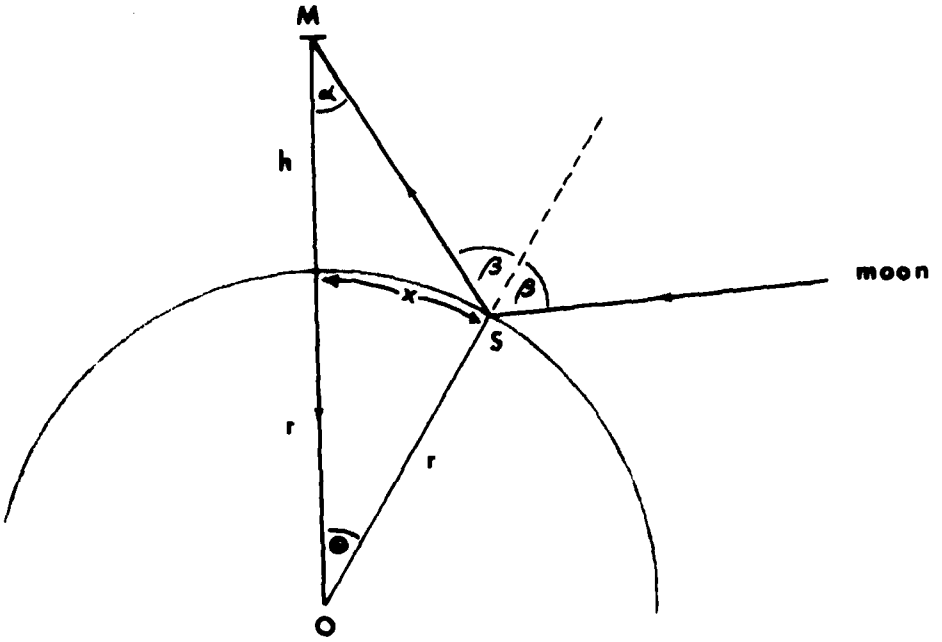

Figure 2. Geometry used to calculate apparent payload rotation rate from lunar reflections on surface.

FILM SENSITIVITY CALIBRATION

Processing of the Eastman Kodak 2475 has been described in the preliminary report on the camera experiment (Ref 1). A $\frac{1}{2}$ sec sensitometer exposure duration was used to match the nominal shutter-open time and so eliminate reciprocity failure effects. The low intensity end of the H&D curve given in Figure 7 of Ref 1 is repeated here in Figure 3 with absolute values of log exposure. The gamma, or mean slope, is 1.26 in the straightline portion of the curve between absolute log E values of -1.72 and -0.21. Film exposure (erg cm^{-2}) in each calibration step is the product of the known sensitometer irradiance (8.0 erg cm^{-2} sec^{-1}), transmission of the appropriate step of the Kodak tablet, and the exposure time ($\frac{1}{2}$ sec).

Although the film was developed in a continuous processing machine (by a commercial developer), fog density was found to vary both along and across the roll. In particular the density was 0.01 to 0.02 greater between the perforations than in the center of the film, an effect believed to be due to turbulence in the developer generated by the perforations when passing through the developing solution. Along the film, variations of 0.01 density unit were sometimes found across distances as small as six inches. For these reasons a density change of 0.02 was considered to be the minimum that could meaningfully be related to luminescence in the plasma around the rocket or to fluorescence on the vehicle skin.

The calibration indicates that we should see a density ~0.02 above fog for the exposure of calibration step 18, i.e. for $E \approx 10^{-2.04} \approx 9 \times 10^{-3}$ erg cm^{-2}, or an irradiance I of 1.8×10^{-2} erg cm^{-2} sec^{-1} during a $\frac{1}{2}$ sec exposure. The exposure E (in erg cm^{-2}) is related to scene brightness B (erg cm^{-2} s^{-1} $ster^{-1}$) by

$$E = It \approx \frac{\pi}{4} \frac{BTt}{f^2} \frac{1}{(1+m)^2}$$

or

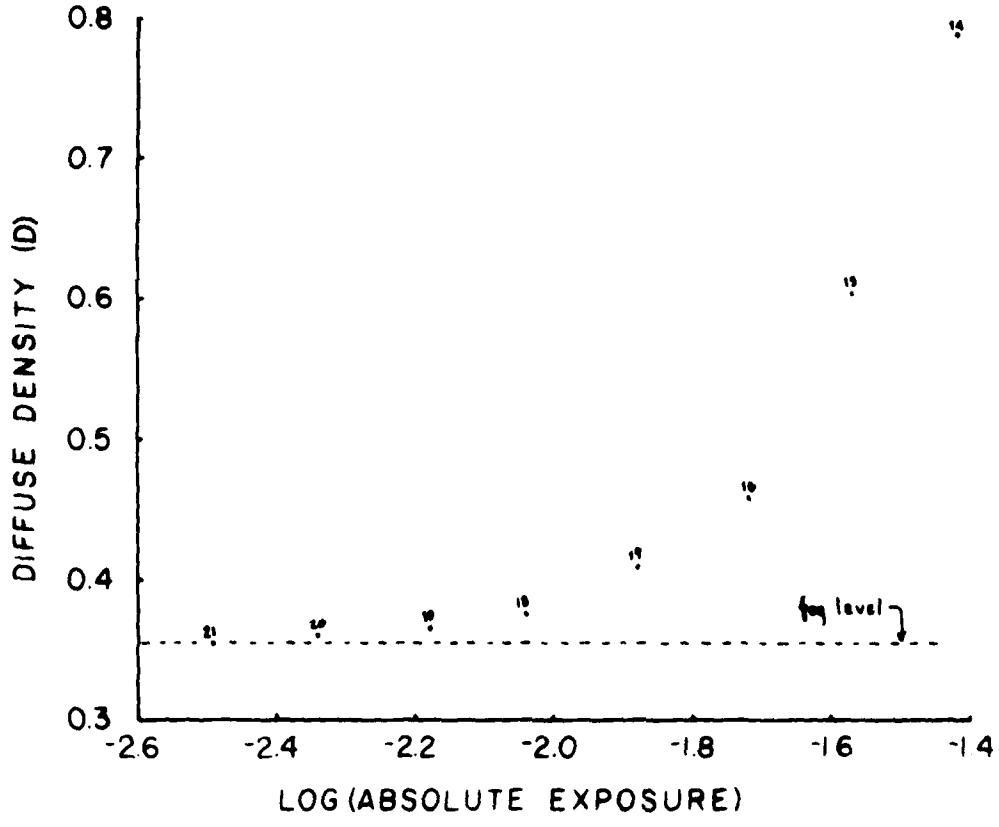

Figure 3. Log exposure part of the D-Log E curve of the film exposed on board AFGL rocket A31-603. Exposure units are erg cm^{-2}.

$$B = \frac{4I f^2 (1 + m)^2}{\pi T}$$

where T = optics transmission, f = lens f-number and m = magnification. In this case f = 1.4, T ≈ 0.9, m ~ 1/100 for the forward field of view and 1/16 for the image of the electrodes on the rocket skin.

Thus, a half second exposure in the forward-directed part of the field of view should give a detectable density for a brightness

$$B \gtrsim 1.8 \times 10^{-2} \cdot 4 \cdot (1.4)^2 \cdot (1 + \frac{1}{100})^2 / (\pi \cdot 0.9), \quad \text{or}$$

$$\underline{B \gtrsim 5.2 \times 10^{-2}} \text{ erg cm}^{-2} \text{ sec}^{-1} \text{ ster}^{-1} .$$

This is equivalent to

$$\frac{4\pi}{10^{-6}} \times 5.2 \times 10^{-2} \times \frac{\lambda}{hc} \text{ rayleighs} \approx \underline{160 \text{ kR}} .$$

Detection of fluorescence on the vehicle skin in the vicinity of the insulating ring would require a scene brightness

$$B \gtrsim 1.8 \times 10^{-2} \cdot 4 \cdot (1.4)^2 \cdot (1 + \frac{1}{16})^2 / (\pi \cdot 0.9), \quad \text{or}$$

$$\underline{B \gtrsim 5.7 \times 10^{-2}} \text{ erg cm}^{-2} \text{ sec}^{-1} \text{ ster}^{-1} .$$

FILM DENSITY MEASUREMENTS

The original objectives of the photographic experiment were to record arcing, if any, between electrodes embedded in the insulator ring on the rocket, and to determine the volume emission rate of luminescence excited in the payload sheath by returning ions or electrons during the flight. In this study we have also considered the possibility of fluorescence excited by charged particles striking the payload surface. The printed lists of telemetered data supplied

by AFGL included measurements from two thermal emission probes giving vehicle potential with respect to the ambient plasma. This information was used to select film frame sequences at times of vehicle potential and accelerator conditions at which discharges would be most probable, in particular times of rapidly changing potential.

Film sequences thus selected were then examined with a MacBeth densitometer to determine what exposure might have resulted from a beam-plasma discharge in the sheath or from fluorescence on the skin. As chemical fog in unexposed areas was found to vary both along and across the film, measurements of fog density were made on the leader and trailer and in those frames exposed when the camera ran in cine mode. There were sufficient such sequences for fog measurements to be made physically close to each region of interest. As the density of most $\frac{1}{2}$ sec exposures was very close to that measured on unexposed film, the density in the 1/24-sec cine exposures was considered an accurate representation of chemical fog density.

Density measurements were made at the edge of the forward field of view (between the sprocket holes) in the center of the forward field, and on the image of the insulator band. In those frames when this band was not visible, i.e. when it was not illuminated by the moon, density readings were taken at approximately the same point in the frame. Fog density measurements were made in an identical manner. The three density values for each frame measured are included in the data list given in Appendix A and a summary of experimental parameters (time, accelerator mode, net emitted current and vehicle potential) is presented in Table 2 with comments on the film density readings. In Table 2, a positive current indicates ion emission and a negative current indicates electron emission, achieved by biasing the beam neutralizer filament.

Six film frame sequences were examined but no change of film density could be found to give any correlation with changes in accelerator operation on payload potential. In some sequences

Table 2. Summary of film density measurements for selected particle beam currents and vehicle potential changes

Time	Mode	Beam Current, μA	Vehicle Potential, Volts	Comments
101.454	10	0	-17	Throughout this sequence
101.954	11	0	-17	there was no detectable
102.456	12	0	-19	density above fog
102.958	1	192	-633	
103.329	2	192	-634	
103.788	3	375	-1033	
104.048	8	0	-47	
113.933	11	-2134	245	Scattered moonlight
114.435	12	-2189	276	steadily increasing,
114.936	1	-652	147	but no detectable
115.276	6	-861	197	changes at times of
115.772	7	15	-544	potential changes
116.274	8	0	-74	
116.772	9	0	-80	
117.276	10	0	-79	
129.302	5	18	-428	Measured density
129.772	6	-9951	65	within 0.01 of fog
130.273	7	12	-446	level, variations
130.776	8	0	-60	$\lesssim$ 0.005, not correl-
131.277	9	0	-60	ated with potential changes
130.074	5	18	-394	Film densities within
135.576	6	~-9932	83	$\lesssim$ 0.005 of fog level
136.078	7	11	-334	
136.578	8	0	-31	
138.585	12	0	-27	Scattered moonlight in
139.085	1	11	-257	forward field. See
139.587	2	10	-251	Fig 4(a)-(c) and text for
140.089	3	15	-277	modes 2, 6, 8. Scattered
140.460	4	16	-269	moonlight gradually de-
140.924	5	16	-250	creased, disappeared
141.467	6	-9900	90	by mode 5.
141.968	7	10	-210	
142.470	8	0	-18	
168.455	2	-10296	60	Electron emission from
168.957	3	-10297	62	neutralizer (~10 ma to 0)
169.459	4	-10292	61	
169.959	5	-1541	30	No detectable density
170.461	6	-2365	18	above fog
170.962	7	0	2	
171.464	8	0	1	

evidence of diffuse illumination was found in the forward-looking field, represented by a density only about 0.01 above the local fog level. One example of this is shown in Figure 4(a), an iso-density plot of the frame taken at time 139.587 (emitted ion current 10μA, rocket potential – 250 volts). Spot density readings in the region of higher density in the sequence of frames about this time showed no detectable change in the image characteristics at the time of ion accelerator burn-on one second earlier. Rocket potential, from thermal emission probe data, changed from -27 volts to -257 volts at turn on (MODE 12 to MODE 1 transition). The isodensity plot is from the frame for MODE 2.

This small density enhancement is characteristic of frames recorded about the times that the moon illuminated the rocket skin in the rearward field of view. It occurred for a longer period than the actual specular reflections from which payload spin rate was determined. The extra exposure due to scattered moonlight should in fact increase the sensitivity of the film because it raises the overall exposure to a more steeply sloped part of the Density-log E curve. However, the slope of the D-log E curve for a density of 0.01 above fog is still only about 0.07, calculated from the values for wedge steps 18 and 19 on the film. Using this as an approximation to the slope of the curve where D is 0.01 above fog, as at step 19, the exposure E required for a further increase of 0.01 in density is a further 2.5×10^{-3} erg cm^{-2}, corresponding to approximately 45 kR.

To raise the film density to 0.01 above fog initially requires about the same exposure as for calibration step 19, i.e. $\sim 6.6 \times 10^{-3}$ erg cm^{-2} which, in a $\frac{1}{2}$ sec exposure, requires a scene brightness of the order of 120 kR. As the slope is very small in this region of the D-log E curve, and is continually changing, the errors in this estimate may be as high as a factor of two.

As no detectable density changes were found coincident with changes in accelerator operation on payload potential, we may conclude that charged particle impact excited fluorescence around the

rocket contributed less than about 45 kR to the optical radiation viewed by the camera.

Figures 4(b) and (c) are isodensity plots of frames recorded during modes 6 and 8 respectively of this sequence. The scattered moonlight component in the forward field had disappeared by this time and the entire forward field is at fog density in both these frames. In Figure 4(b) there is actually a slight decrease of ~0.1 in density at the position of the insulator band in the lower part of the frame.

In Figure 4 captions:

i = beam current

V = potential of the rocket with respect to the ionospheric plasma.

MODE refers to the mode of operation of the accelerator system as explained in Table 4 of Ref 3.

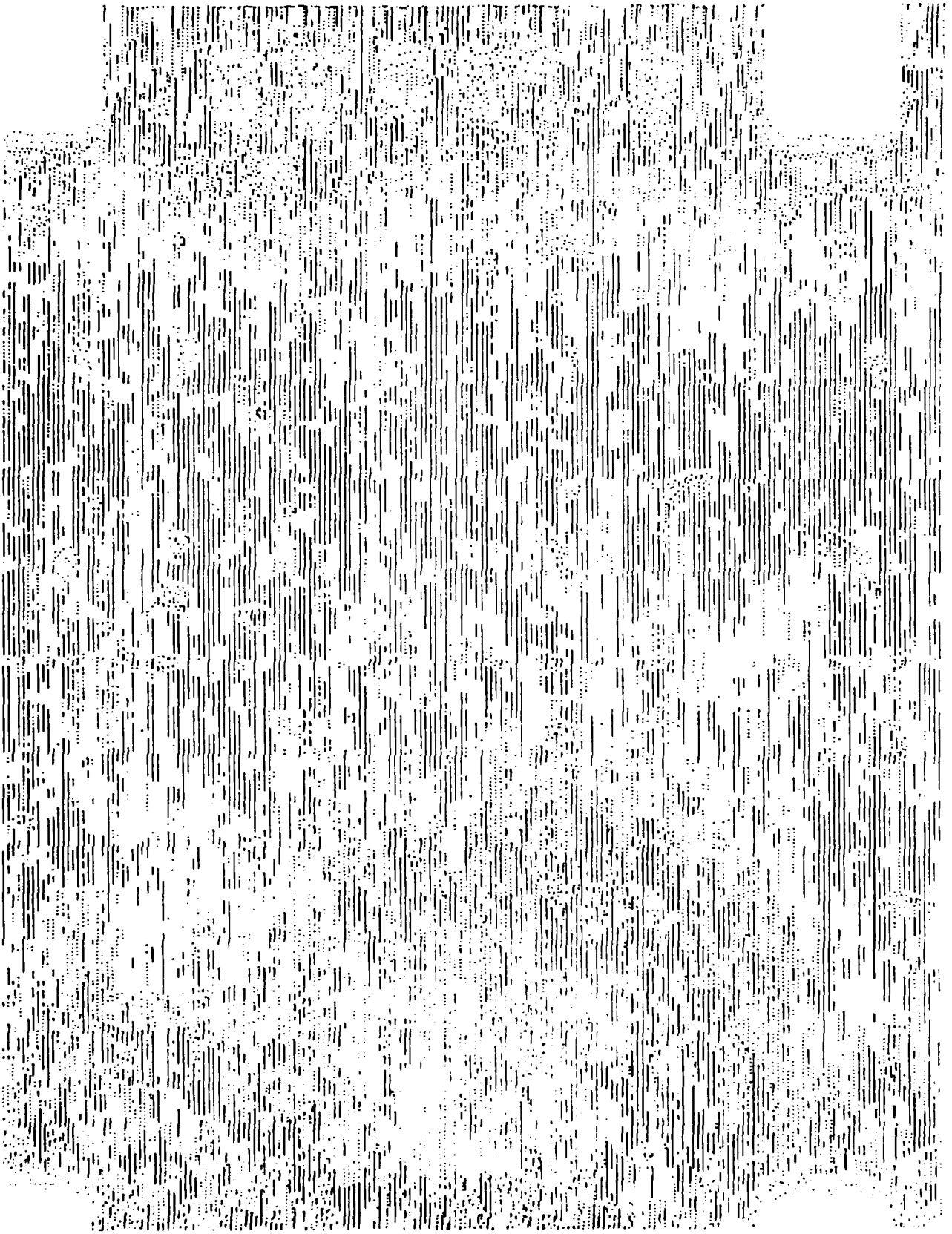

Figure 4(a). Scanning microdensitometer plot of frame exposed at flight time 139.587 sec from launch MODE 2, i = 10μA, V = - 251 volts; contour interval $\Delta D \sim 0.004$ between symbols.

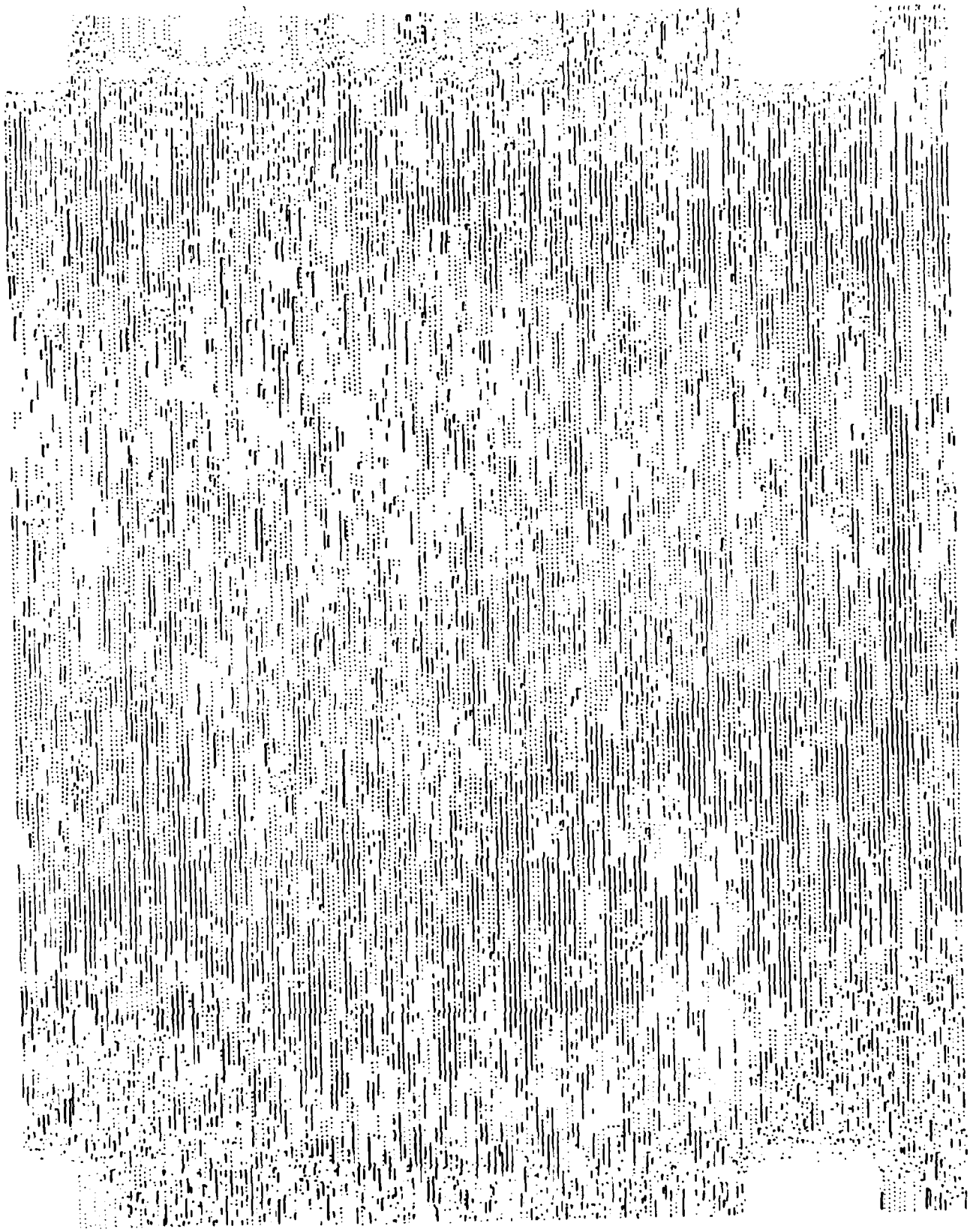

Figure 4(b) Scanning microdensitometer plot of frame from 141.467 sec from launch. MODE 6, i = -9.9 mA, V = +90 volts; contour interval $\Delta D \sim 0.004$ between symbols.

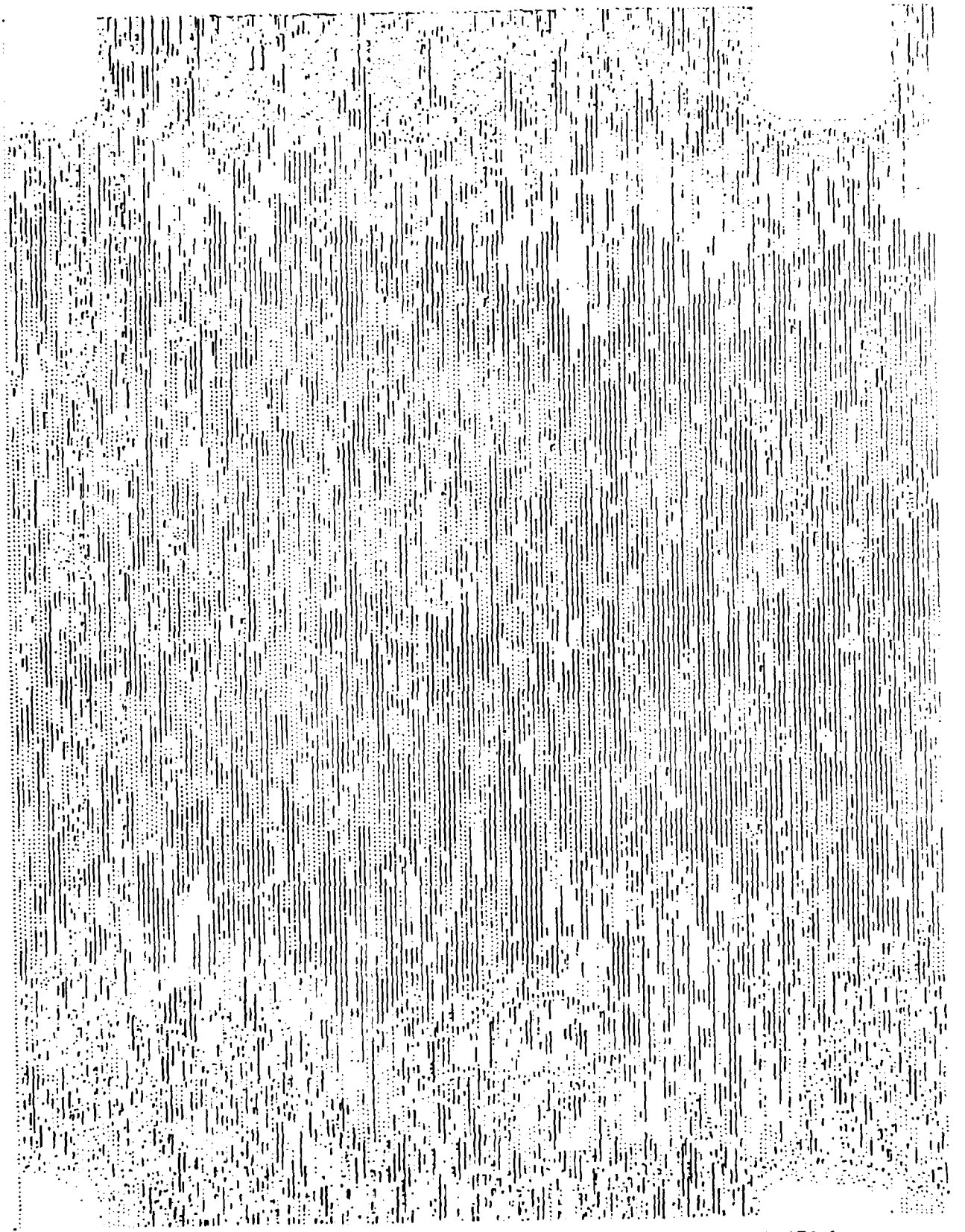

Figure 4(c) Scanning microdensitometer plot of frame from 142.470 from launch. MODE 8, i = 0, V = -18 volts; contour interval $\Delta D \sim 0.004$ between symbols.

SECTION III

THEORETICAL CONSIDERATIONS, INTERPRETATION

SHEATH DIMENSIONS

To estimate the dimensions of the plasma-depleted sheath surrounding the rocket, we use the concentric-spherical approximation of Ref 5. The ratio of the distance to the external "electrode" r_o to the characteristic dimension of the rocket r (19 cm) is then given by the parametric equation

$$i = 4\pi\, 2.3 \times 10^{-6}\, \frac{V^{3/2}}{\alpha(r_o/r)^2} \quad \text{for electrons}$$

$$= 4\pi\, \frac{5.45 \times 10^{-8}}{\sqrt{M}}\, \frac{V^{3/2}}{\alpha(r_o/r)^2} \quad \text{for ions of molecular weight M .}$$

The procedure is to determine α^2 from the emitted current i resulting in charge-up voltage V measured by the onboard instruments, from which the ratio r_o/r is found in Table II of Ref 5.

For a return current of 10μA of <u>ions</u> of atomic weight 16 and a charge-up voltage 250 volts $\alpha(r/r_o)^2 = 67.7$, for which $r_o/r \approx 17$ and hence $r_o \approx 323$ cm. This value will apply above about 200 km where $^{16}O^+$ is the dominant ion in the ionosphere. For molecular weight 30 α^2 is 49.4; an interpolation in Table II of Ref 5 gives $r_o/r = 14$ and hence $r \approx 266$ cm. This value will apply below about 200 km where NO^+ is the dominant ion.

For a return current of 10 mA of <u>electrons</u> at a charge-up voltage of 100 volts, this approach gives a sheath radius of about 60 cm, which is less than the length of the rocket. This case was therefore recalculated using the cylindrical approximation of Ref 6:

$$i' = 14.68 \times 10^{-6}\, V^{3/2}/r\beta^2 ,$$

where i′ is in amperes/cm and β a geometric parameter analogous to the function α above. Thus $i' = 10^{-5}/300$ (the rocket length ℓ is 300 cm), and $r/\beta^2 = 440$. As r = 19 cm, $\beta^2 = 23.2$; interpolation in Table III of Ref 6 gives $r_o/r = 7.7$, so that $r_o = 146$ cm, which gives a sheath thickness of 127 cm.

The sheath dimensions, as calculated here, are independent of the ionosphere plasma densi or temperature except for the choice of ion mass number which depends on the identity of the dominant ion.

RADIATION DENSITIES

We considered next the excitation of air by 10 mA of 100 eV electrons returning through the cylindrical sheath of surface area $A = 2\pi R\ell$. At the typical rocket altitude of 150 km ambient N_2 density $n(N_2)$ is 2×10^{12} cm^{-3}. The electron impact cross section σ for the First Negative system of N_2^+ is about 10^{-17} cm^2 near 100 eV. The viewing mirror is 15 cm from the rocket surface and looks parallel to the rocket axis, so that R = 15 + 19 = 34 cm and ℓ = 300 cm. The volume emission rate in the line of sight will be $(i/eA)\,\sigma n(N_2 \approx 2.8 \times 10^7$ photons cm^{-3} sec^{-1} (e is the electronic charge). The length of the line of sight within this emitting region is $\sim$200 cm, so the column emission rate is 6×10^9 photons (cm^2 column)$^{-1}$ or 6 kilorayleighs.

This brightness is far lower than the detection threshold of this experiment. Further contributions may be expected from other emission features (principally, the First and Second Positive systems of N_2), but as these will probably result in an increase of less than a factor of two the main conclusion is not changed. Further, the ends of the cylindrical sheath have been neglected in the calculation; the sheath will in fact extend beyond the ends of the vehicle and as a result be slightly thinner than calculated here but again the expected emission rates will change only slightly.

At higher rocket altitudes the concentrations of N_2 and O will be lower and so the expected emission rates will be still lower.

For positive ions returning to a negatively charged rocket, the surface radiances will be still lower: cross sections for excitation of visible radiation by ion impact at the energies of only a few hundred electron volts are small, and in addition the ion current density is some orders of magnitude less than that of the electrons.

If an electronic discharge occurs, most of the returning energy will be dissipated in the sheath. For a discharge with input power equivalent to 10 mA at 100 V, in which the total visible fluorescence efficiency is ϵ, the volume emission rate in a cylindrical sheath of radius r_o about a vehicle of (inner) radius r and length ℓ will be

$$\frac{Vi}{\pi \ell (r_o^2 - r^2)} \epsilon \text{ watts cm}^{-3} \text{ sec}^{-1} .$$

With the above conditions r_o = 146 cm, r = 19 cm, and ℓ = 300 cm, and adopting ϵ = 0.02, this become 10^{-9} watts cm^{-3} sec^{-1} or $\sim 2.5 \times 10^9$ photons cm^{-3} sec^{-1}. Taking again the above camera line-of-sight distance of 220 cm, the radiance is 5.6×10^{11} photons $(cm^2 \text{ column})^{-1}$ sec^{-1} or 560 kilorayleighs, which would have produced a density about 0.32 above fog in the rocket experiment.

Again neglect of the effects of the ends of the sheath is not expected to change the overall conclusion, which is that an electric discharge excited during electron emission in this experiment should have produced a film density greater than any actually recorded. It should be noted that small changes in the current output have only a small effect on the surface brightness of the discharge (the decrease in total energy input is compensated by a decrease in the radius of the sheath; the volume emission rate therefore stays about the same, and as the path length is unchanged the surface brightness is also unchanged).

A discharge during emission of 10μA of ions for an effective charge-up potential of 250 volts may be expected to produce a total emission of $10 \times 10^6 \times 250 \times 0.02 \times \frac{\lambda}{hc} \approx 1.3 \times 10^{14}$ photons sec^{-1} (again adopting the plausible ϵ = 0.02). If this radiation is produced

in a volume of the order of the sheath size determined above the average volume emission rate will be $\sim 10^6$ photons cm^{-3} sec^{-1}. The length of the path seen by the camera through this spherical discharge region will be about 4 meters so that the apparent brightness will be of the order of $10^6 \times 4 \times 10^2 \approx 4 \times 10^8$ photons $(cm^2 \text{ column})^{-1}$ sec^{-1} or $\sim \frac{1}{2}$ kR. This radiance would not be detected by the camera system.

RADIATION EXCITED AT THE ROCKET SURFACE

We estimate next the surface radiance of the rocket's skin that results from fluorescence excited by counterflowing energetic electrons or ions. This radiance can be expressed as

$$f \frac{1}{\pi} Vi/A,$$

where i is the return current flow through the sheath at potential difference V, A is the skin surface area over which this current is distributed (the current density i/A is assumed uniform), f is the effective fluorescence efficiency of the skin material in the visible (and near-UV and -IR wavelengths at which commonly used photodetectors are sensitive), and the factor $1/\pi$ as usual converts the total output flux to the flux per steradian in the direction normal to the surface. The factor iV/A will be recognized as the power deposited per unit area of skin by the impinging particles; we have neglected the small loss (see previous subsection) from their excitation of atoms and molecules within the sheath, and assumed no beam plasma discharge is taking place.

Following the argument in the previous subsection, we take as standard conditions i = 10 ma, V = 100 volts, and A = $2\pi \times 19$ cm x 300 cm = 3.6×10^4 cm^2 (end plates neglected). The power density iV/A is then 1 watt/3.6×10^4 $cm^2 \approx 28 \mu w/cm^2$, and the surface radiance is $28 \times 10^{-6} f/\pi$ watts/(cm^2 sterad) or $280 f/\pi$ erg/(cm^2 sec). As Fig 3 shows, the threshold exposure of our (fast) photographic film is about 10^{-2} erg/cm^2, so that for detection in a 1-sec exposure with an f/1.4 lens

$$\frac{\pi}{4} \cdot \frac{280 f}{1.98 \pi} > 10^{-2}, \quad f > 3 \times 10^{-4} .$$

In practice the fluorescent yield of clean metals is many orders of magnitude less than 10^{-4}, so that the "cathodoluminescence" at metal surfaces would be far below photographic threshold. In addition, none of the partially-conducting plastic materials on the surface, or the oxide film or aluminum, would be expected to have efficiencies as high as 10^{-4}. Thus no electron bombardment-induced surface fluorescence would be expected in onboard photography images of A31.603. As yield under bombardment by $\sim$ 250 eV ions are even lower, no ion-induced surface fluorescence would be detectable either (efficiencies of $\sim$25% would be required for the 10μA beam to be above threshold).

On the other hand, conventionally-used phosphor materials – such as ZnS and alkali halides – have efficiencies for visible and near-UV emission between 10^{-1} and 10^{-2} under irradiation by sub-kilovolt electrons (Ref 7). Hence phosphor coatings – and perhaps even luminescent paint – applied to the rocket surface would "map" the spatial distribution of return electron-beam power at the levels of power-per-unit-area of these calculations.

Additionally, the transverse currents in pn junction semiconductors induced by the returning electrons (Ref 8) can be used to map out the energy distribution. The basic instrument is a simple diode biased at a few volts, with a current amplifier. As each 100 eV electron creates $\sim$10 hole-electron pairs, the collected current in a 1 cm^2-area diode would be

$$\frac{10^{-2} \text{ amps}}{36000 \text{ cm}^2} \cdot 10 \approx 3 \text{ microamps} .$$

(It is worth noting that both the electron beam-induced currents and luminescence concepts are in routine use in electron microscopy for mapping surface distributions.)

SUMMARY AND RECOMMENDATIONS

The main results of this study may be summarized as follows:

1. Each frame on the film has been unambiguously itentified with respect to time and operation of the particle accelerators.

2. Determination of rocket aspect from lunar reflections off the skin was only partially successful due to the nature of the skin surface. The reflections permitted location of the moon, relative to the rocket, to within the plane quadrant defined by the vehicle's rearward axis and the radius vector through the mirror mount.

3. Lunar reflections from the rocket surface were used to determine an apparent rotation rate about the longitudinal axis of $\frac{1}{71}$ sec^{-1}, which differed from that derived from magnetometer data ($\frac{1}{23}$ sec^{-1}) but which might be useable in further clarifying the aspect information from the magnetometers.

4. Detection threshold for air fluorescence has been determined to be ~ 160 kR for film density 0.02 above fog.

5. Microdensitometric examination of the film revealed no density changes which could not be attributed to scattered moonlight and none which could be related to changes in vehicle potential or accelerator operation. Densities in aeras not exposed to moonlight were generally within 0.01 of fog levels.

6. Calculations of expected fluorescence in the ambient plasma due to particle ejection and vehicle charging indicate that no visible radiation would have been detected during ion or electron ejection in the absence of a discharge. Radiation should have been detected in the prescence of discharges when the electron accelerator was on and vehicle potential was of the order of 100 volts.

7. Surface-excitation efficiencies needed for detection of charged particle impact fluorescence on the rocket skin have been calculated as $\gtrsim 3 \times 10^{-4}$ for the electron emission conditions. As metals and other rocket surface materials have much lower fluorescence efficiencies, no detectable surface radiation is expected. On the other hand, fluorescent material placed on the rocket surfaces should readily "map" the return current distribution.

REFERENCES

1. R.B. Sluder and I.L. Kofsky, Photographic Measurements of Electrical Discharges, AFGL-TR-78-0082, 31 Mar 78.

2. R.B. Sluder and I.L. Kofsky, Equipment Information Report on F19628-77-C-0124, PhotoMetrics, Inc., 15 Nov 77.

3. W. Huber, Design Fabricate and Test Instrumentation for Rocket-borne Measurements of Vehicle Charging, AFGL-TR-78-0164, 19 Jun 78.

4. R.B. Sluder and I.L. Kofsky, Design Evaluation Report on F19628-77-C-0124, PhotoMetrics, Inc., 15 Nov 77.

5. I. Langmuir and K. Blodgett, Currents Limited by Space Charge Between Concentric Spheres, Physical Review Vol XX III, 49, 1924.

6. I. Langmuir and K. Blodgett, Currents Limited by Space Change Between Coaxial Cylinders, Physical Reviews, Vol. XX II, 347, 1923.

7. H.R. Luxenberg and R.L. Kuehn, Display Systems Engineering McGraw-Hill, N.Y. 1968, Chapter 8.

8. P.R. Thornton, Scanning Electron Microscopy, Chapman and Hall, London 1968, Chapter 9.

APPENDIX A

16 mm Film Listing from AFGL Rocket A31.603

All data frames on the film from the 16 mm camera flown on rocket A31.603 are listed here. The list identifies MODE and CYCLE codes from film, decoded mode numbers, film footage numbers (numbered every $\frac{1}{2}$ foot), flight time after launch in seconds, exposure times, and densitometer readings.

Film Footage Numbering

Footage is indicated on the film by a 5 digit number every 6 inches. In the list, the number is listed with the frame at the position of the two least-significant digits; the other three digits are at the edge of an adjacent frame. In most cases only the two least significant digits are listed. The numbers are in descending order, i.e., the film was run backwards through the camera.

Timing

Times given here and on the reduced telemetry record are times from launch in seconds. Some telemetry seconds have time of day in seconds (Z). Launch time was 0900 Z + 1 sec = 32401 Z; subtracting this number from the time of day gives time of flight from launch. The exposure time of each frame is listed in milliseconds.

Footage Number	Mode Code	Mode	Cycle Code	Cycle	Time	Exposure Time	Densities Edge	Densities FWD	Densities Skin	
	03	4	0200	3	95.350	502				
	04	5	0200		95.852	502				
	05	6	0200		96.354	502				
	10	7	0200		96.856	502				
	11	8	0200		97.358	500				
	12	9	0200		97.858	502				
	13	10	0200		98.360	502				
	14	11	0200		98.862	374				
		5			99.236	211	Not on Film			
	05	6	0200		99.447	502				
51351	10	7	0200		99.949	502	.320	.310	.310	
	11	8	0200		100.451	501	.320	.305	.310	
	12	9	0200		100.952	502	.320	.310	.310	
	13	10	0200		101.454	500	.320	.310	.310	
	14	11	0200		101.954	502	.320	.310	.310	
	15	12	0200		102.456	502	.320	.310	.310	
	00	1	0300	4	102.958	502	.320	.310	.310	gun started
	01	2	0300		103.329	371				
	02	3	0300		103.788	459	.320	.310	.310	
	11	8	0300		104.048	260	.320	.320	.310	
	12	9	0300		104.539	491	.320	.310	.310	
	13	10	0300		105.041	502	.320	.310	.310	
	14	11			105.543	501				
	15	12	0300		106.044	502				
		1			106.546	033	Not on Film			
	02	3	040&							
	02	3	040&							
	02	3	040&				.320	.310	.305	
	02	3	040&							
	02	3	040&		106.579	408	.320	.310	.310	fog densities
	02	3	040&				.320	.310	.310	
51350	02	3	040&							
	02	3	040&							
	02	3	040&							
	02	3	040&							
	05	6	040&		106.987					
	05	6	0400							
	16		0400		107.110					
	03	4	0000	1	107.367					
	03	4	010&	2	12 frames					
51349	04	5	0100	2	108.216	502	.330	.320	.315	thermal emission
	05	6	0100		108.718	432	.330	.315	.310	probe #1 to lower
	01	2	0100		109.150		.320	.315	.310	potential, 108.180
					11 frames					fog densities
	02	3	0100							
	02	3	0100							
	06	?	0100							
	06	?	0100							
	14	?	010&		3 frames					
51348	14	?	010&							
	14	?	010&		7 frames					
	15	12	0100							
	01	2	010&		6 frames					

Footage Number	Mode Code	Mode	Cycle Code	Cycle	Time	Exposure Time	Densities Edge	FWD	Skin	
	07	?	010&		5 frames					
47	07	?	010&				.340	.320	.325	fog densities
	07	?	010&		4 frames					
	12	9	0000		112.013	429				
	11	8	0100		112.442	491				
	12	9	0100		112.933	500				
	13	10	0100		113.433	500				
	14	11	0100		113.933	502	.355	.340	.330	+ 245 scattered
	15	12	0100		114.435	501	.355	.340	.330	+ 276 moonlight
	00	1	0200	3	114.936	340	.350	.340	.330	+ 147
	05	6	0200		115.276	496	.355	.345	.330	+ 197
	10	7	0200		115.772	502	.350	.355	.330	- 544
	11	8	0200		116.274	498	.350	.355	.330	- 74
	12	9	0200		116.772	504	.360	.360	.335	- 80
	13	10	0200		117.276	502	.360	.360	.330	- 79
	14	11	0200		117.778	501				
	15	12	0200		118.279	502				
	00	1	0300	4	118.781	502				
46	01	2	0300		119.283	503				
	02	3	0300		119.786	076				
	05	6	0300		119.862	467				
	10	7	0300		120.329	500				
	11	8	0300		120.829	502				
	12	9	0300		121.331	502				
	13	10	0300		121.833	502				
	14	11	0300		122.335	500				
	15	12	0300		122.835	502				
	00	1	0400	5	123.337	502				
	01	2			123.839	502				
	02	3	0400		124.341	498				
	01	2	0000	1	124.839	463				moon
	06	?	0000		125.302	501				
	07	8	0000		125.803	503				
	12	9	0000		126.306	114				
	15	12	0000		126.420	211				
					126.631	468	Not on Film			
	02	3	0100	2	127.099	501				
	03	4	0100		127.600	3[illegible]9				
	12	9	0100		127.969					
	16	?	010&							
	16	12 ?	010&		.0 frames		.350	.335	.335	fog densities
	17	-	010&							
	17	-	0100		128.354	637				
	02	3	0200	3	128.991	246				B10
	03	4	0200		129.237	065				
	04	5	0200		129.302	470	.350	.340	335	428
	05	6	0200		129.772	501	.350	.340	.335	-65
	10	7	0200		130.273	503	.350	.345	.335	446
	11	8	0200		130.776	501	.355	.345	.335	60
	12	9	0200		131.277	500	.350	.340	.330	60
44	13	10	0200		131.777	502				
	14	11	0200		132.279	501				

Footage Number	Mode Code	Mode	Cycle Code	Cycle	Time	Exposure Time	Densities Edge	FWD	Skin	
	15	12	0200		132.780	502				
	00	1	0500	6	133.282	502				
	01	2	0500		133.784	500				
	02	3			134.284	331				
	03	4	0500		134.615	459				B10
	04	5	0500		135.074	502	.370	.360	.340	+394
	05	6	0500		135.576	502	.370	.360	.330	- 83
	10	7	0500		136.078	500	.360	.360	.340	+334
	11	8			136.578	502	.365	.365	.340	+ 31
	12	9			137.080	502				
	13	10			137.582	502				
	14	11			138.084	502				
	15	12			138.585	501	.340	.340		
	00	1	0600	7	139.085	500	.340	.340		
	01	2	0600		139.587	502	.355	.340	.330	
	02	3	0600	7	140.089	371				
	03	4	0600		140.460	464	.360	.335	.330	
	04	5	0600		140.924	543	.360	.335	.330	
43	05	6	0600		141.467	501	.360	.335	.330	
	10	7	0600		141.968	502	.360	.340	.335	
	11	8	0600		142.470	502	.360	.340	.335	
	12	9	0600		142.972	500	.360	.340	.330	
	13	10	0600		143.472	502	.360	.335	.330	
	14	11	0600		143.974	501				
	15	12	0600	7	144.475	502				
	00	1	0700	8	144.977	502				
	01	2	0700		145.479	500				
	02	3	0700		145.979	265				
	03	4	0700		146.244	613				
	04	5	0700		146.857	500				
	05	6	0700		147.357	175				
	13	10	070&		12 frames					
42	13	10	070&		147.532	495	.360	.340	.340	fog densities
	14	11	0700		148.027	264				
	15	12	0700		148.293	260				
	00	1	1000	9	148.553	277				
	01	2	1000		149.030	500				
	02	3	1000		149.530	419				
	03	4	1000		149.949	316				
	04	5	1000		150.365	377				
	05	6	1000		150.742	492				
	16	?	0000	1	151.234					
	17	12	0000	1						
	02	3	0100	2	151.684	599	.380	.365	.340	
	03	4	0100		152.283	422	.380	.350	.340	
	04	5	0100		152.705	069	.370	.350	.340	fog level
	11	8	0100		152.774	406	.380	.355	.350	
	00	1	0000	1	153.180	237	.370	.350	.350	scattered moonlight
41	01	2	0000	1	153.417	500	.385	.370	.360	varying exposure
	02	3	0000		153.917	502	.390	.370	.360	times
	03	4			154.419	502	.390	.380	.360	
	04	5			154.921	500				

Footage Number	Mode Code	Mode	Cycle Code	Cycle	Time	Exposure Time	Densities Edge	Densities FWD	Densities Skin	
	05	6	0000	1	155.421	503				B8 up at 155.951
	10	7	0000		155.924	503				
	11	8	0000		156.427	500				
	12	9	0000		156.927	501				
	13	10	0000		157.428	502				
	14	11	0000		157.930	500				
	15	12	0000		158.430	502				
	00	1	0100	2	158.932	502				
	01	2	0100		159.300	468	.380	.360	.360	
	02	3	0100		159.768	330	.375	.350	.350	moon
	04	5	010&		160.098	500				
	04	5	0100							
	05	6	0100		160.598	502	.380	.355	.355	
	10	7	0100		161.100	502				
	11	8	0100		161.602	501				
	12	9	0100		162.103	501				
40	13	10	0100		162.605	502				
	14	11	0100		163.107	500				
	15	12	0100		163.607	502				
	00	1	0200	3	164.109	502				
	01	2			164.611	501				
	02	3			165.112	262				
	03	4			165.374	491				
	04	5			165.865	500				
	05	6			166.365	342				
	10	7			166.707	299				
	02	3	030&	4	167.006					B8 down at
					5 frames					167.375
	03	4	030&							
	03	4	0300							
	05	6	030&		3 frames					
39	05	6	030&				.380	.355	.355	fog
	05	6	030&		7 frames					
	05	6	000&	1?						
	11	8	000&		7 frames		.380	.350	.340	fog
	10	7	040&	5?		on film but not on list?				
	00	1	0400		168.226	229				
	01	2	0400		168.455	502	.365	.345	.345	
	02	3	0400		168.957	502	.360	.340	.340	
38	03	4	0400	5	169.459	500	.360	.340	.340	
	04	5	0400		165.959	502	.360	.340	.340	B8 up at
	05	6	0400		170.461	501	.360	.340	.340	170.212
	10	7	0400		170.962	502	.360	.340	.340	
	11	8	0400		171.464	502	.360	.340	.340	
	12	9	0400		171.966	500				
	13	10	0400		172.466	502				
	14	11	0400		172.968	500				
	15	12	0400	5	173.468	502				
	00	1	0500	6	173.970	501				
	01	2			174.471	502				
	02	3			174.973	168	.370	.340	.340	
	04	5	050&		6 frames	149	.36-.38	.340	.340	fog
	05	6	0500		175.390	502	.360	.340	.340	
	10	7	0500		175.892	501				

Footage Number	Mode Code	Mode	Cycle Code	Cycle	Time	Exposure Time	Densities Edge	Densities FWD	Densities Skin
37	11	8	0500		176.393	503			
	12	9	0500		176.896	501			
	13	10	0500		177.397	502			
	14	11	0500		177.899	498			
	15	12	0500	6	178.397	502			
	00	1	0600	7	178.899	501			
	01	2	0600		179.401	501			
	02	3	0600		179.902	268			
	09	4?	0600		180.170	045			
	04	5	0600		180.215	481			
	05	6	0600		180.696	501			
	10	7	0600		181.197	502			
	11	8	0600		181.699	502			
	12	9	0600		182.199	502			
	13	10	0600		182.701	501			
	14	11	0600		183.202	500			
	15	12	0600	7	183.702	502			
	00	1	0700	8	184.204	502			
	01	2	0700		184.706	502			
	02	3	0700		185.708	374			
36	03	4	0700		185.582	378			
	04	5	0700		185.960	500			
	05	6	0700		186.460	502			
	10	7	0700		186.962				
	11	8	0&--		187.359				
	12	9	----						
	12	9	0700						
	13	10	0---						

Camera battery monitor (B4 in telemetry listing) showed a drop to ~0 volts at ~186.960. Remainder of film incomprehensible.

& indicates blurred character, not readable.